An empirical zenith wet delay correction model using piecewise height functions

YiBin Yao[1,2,3], YuFeng Hu[1*]

[1]*School of Geodesy and Geomatics, Wuhan University, 129 Luoyu Road, Wuhan 430079, China.*

[2]*Key Laboratory of Geospace Environment and Geodesy, Ministry of Education, Wuhan University, 129 Luoyu Road, Wuhan 430079, China*

[3]*Collaborative Innovation Center for Geospatial Technology, 129 Luoyu Road, Wuhan 430079, China*

Corresponding to: yfhu@whu.edu.cn

***Abstract*—**Tropospheric delay is an important error source in space geodetic techniques. The temporal and spatial variations of the zenith wet delay (ZWD) are very large, and thus limit the accuracy of tropospheric delay modelling. Thus it is worthwhile undertaking research aimed at constructing a precise ZWD model. Based on the analysis of vertical variations of ZWD, we divided the troposphere into three height intervals: below 2 km, 2 km to 5 km, and 5 km to 10 km, and determined the fitting functions for the ZWD within these height intervals. The global empirical ZWD model HZWD, which considers the periodic variations of ZWD with a spatial resolution of $5°\times5°$, is established using the ECMWF ZWD profiles from 2001 to 2010. Validated by the ECMWF ZWD data in 2015, the precisions of the ZWD estimation in the HZWD model over the three height intervals are improved by 1.4 mm, 0.9 mm, and 1.2 mm, respectively, compared to that of the currently best GPT2w model (23.8 mm, 13.1 mm, and 2.6 mm). The test results from ZWD data from 318 radiosonde stations show that the root mean square (RMS) error in the HZWD model over the three height intervals was reduced by 2% (0.6 mm), 5% (0.9 mm), and 33% (1.7 mm), respectively, compared to the GPT2w model (30.1 mm, 15.8 mm, and 3.5 mm) over the three height intervals. In addition, the spatial and temporal stabilities of the HZWD model are higher than those of GPT2w and UNB3m.

Index Terms—Tropospheric delay, zenith wet delay, vertical variations, height dividing, HZWD model.

1 Introduction

The radio waves experience propagation delays when passing through the neutral atmosphere (primarily the troposphere), which are known as the tropospheric delays. The tropospheric delay is one of the main error source in space geodetic techniques. In the processing of the space geodetic data, the tropospheric delay along the propagation path is generally expressed as the product of zenith tropospheric delay (ZTD) and mapping function (MF). The ZTD is divided into a zenith hydrostatic delay (ZHD) and a zenith wet delay (ZWD) (Davis *et al*., 1985), and the ZHD can be accurately determined using pressure observations. Unlike the ZHD, the ZWD is difficult to calculate accurately due to the high spatio-temporal variation in water vapour. Its spatial distribution is characterized with a near-zonal dependency, with values varying from about 2 cm at high latitudes to about 35 cm near the equator (Fernandes *et al.*, 2013). The temporal variation pattern of ZWD is mainly characterized by the seasonal variability including annual and semi-annual components (Jin *et al.*, 2007; Nilsson *et al.*, 2008). The high viabilities in ZWD make itself the main factor influencing tropospheric delay correction.

Various methods and models are developed to estimate the ZWD. Ray-tracing uses the observations from radiosonde profile (Davis *et al.*, 1985; Niell, 1996) or numerical weather models (Hobiger *et al.*, 2008; Nafisi *et al.*, 2012) to calculate the ZWD. It can provide the most accurate ZWD corrections. Based on the total column water vapour (TCWV) combined with the weighted mean temperature, the single layer model is developed to convert the TCWV to ZWD at the reference height level (Fernandes *et al.*, 2013, 2014; Stum *et al.*, 2011; Vieira *et al.*, 2017). However, this model suffers from the errors associated with the ZWD height variations. The traditional Saastamoinen model (1972) and Hopfield model (1971) approximate the ZWD with surface observations as temperature and water vapour pressure observations. Without the

information about the vertical distribution of water vapour, the stability and reliability of their ZWD estimates are poor. Moreover, both models are highly dependent on meteorological data. The aforementioned models have the limitations of application in wide area augmentation and real-time navigation and positioning. Therefore, the empirical climatological models were proposed as practical conditions required. The RTCA-MOPS (2016), designed by the US Wide Area Augmentation System (Collins et al., 1996), estimates ZWD by using the latitude band parameters table. The modified RTCA-MOPS model − called UNB3m (Leandro, 2006) − uses relative humidity as a parameter instead of the water vapour pressure to calculate the ZWD, effectively improving the precision of ZWD estimation to 5.5 cm (Möller et al., 2014), but the model deviation is increased when the height exceeds 2 km (Leandro, 2006). The TropGrid model (Krueger et al., 2004, 2005) provides the meteorological parameters needed to calculate tropospheric delay in the form of $1° × 1°$ grid. The improved TropGrid2 model (Schüler, 2014) enhances the efficiency of ZWD calculation by directly modelling ZWD with the exponential function. Based on the GPT2 model (Lagler et al., 2013), the GPT2w model (Böhm et al., 2015) adds weighted mean temperature and a vapour pressure decrease factor realised as a global grid to estimate ZWD by using the Askne and Nordius formula (Askne & Nordius, 1987). The GPT2w model has the best precision of ZWD estimation (3.6 cm) compared to other commonly used models (Möller et al., 2014).

The water vapour changes rapidly with respect to height, and the trends in water vapour at different heights vary, so the wet delay with direct relation to water vapour has complex spatio-temporal variations in the vertical direction. Kouba (2008) proposed an empirical exponential model to account for the height dependency of ZWD, but it only be applicable within the height below 1000 m. The aforementioned empirical models are all based on a fixed height (average sea level or surface height) and use only a single decrease factor to describe the variation of water vapour or wet delay with respect to height, which makes it difficult to allow for the vertical distribution differences in water vapour (or wet delay) in the upper troposphere. In the course of aircraft dynamic navigation and positioning, the zenith delay error will result in two

88   times errors in the station height estimate (Böhm and Schuh, 2013). Thus it is necessary

89   to correct the wet delay at different heights, which is clearly difficult for the

90   aforementioned models. Based on the analysis of the characteristics of the ZWD profile,

91   an empirical ZWD model, named HZWD, is established based on three functions

92   applicable within corresponding height intervals, and the model precision is verified by

93   European Centre for Medium-Range Weather Forecast (ECMWF) reanalysis data as

94   well as radiosonde data.

95

2 Vertical variations of ZWD

97   ZWD is defined as the integral of the wet refractivity along the vertical profile

98   above the station:

$$ZWD = 10^{-6} \int_{H}^{\infty} N_w dh = 10^{-6} \int_{H}^{\infty} (k_2' \frac{e}{T} + k_3 \frac{e}{T^2}) dh \tag{1}$$

100   In equation (1), N_w is the wet refractivity; e is the water vapour pressure in hPa;

101   T is the temperature in Kelvin; k_2' is 22.1 K/hPa and k_3 is 373900 K^2/hPa (Bevis *et*

102   *al*., 1994). It can be seen from equation (1) that ZWD changes with height, vapour

103   pressure and temperature. The ZWD will decrease with increasing height due to the

104   shorter integral length. With the profiles of water vapour pressure and temperature, one

105   can obtain the accurate ZWD by ray tracing method. However, in practical applications

106   (*e.g.*, aircraft navigation and positioning, wide area augmentation), we usually uses

107   empirical models for ZWD corrections due to the unavailability of meteorological data

108   profiles. Therefore, it is necessary to develop an empirical ZWD model with high

109   precision. The temperature roughly decreases linearly with increasing height in the

110   troposphere, while the change in water vapour is more variable, so the water vapour is

111   the main determinant of vertical variation of ZWD. In the following content, we used

112   the meteorological data profile of ERA-Interim pressure levels provided by ECMWF

113   to analyse the vertical variation characteristics of ZWD and explore a suitable fitting

114   function capable of describing the changes in ZWD with respect to height.

115   ERA-Interim can provide data at 0:00, 6:00, 12:00, and 18:00 UTC daily with a

116 spatial resolution of not more than $0.75\degree \times 0.75\degree$ and 37 pressure levels (Dee *et al.*,

117 2011). The highest level data come from a height of approximately 50 km, covering

118 almost the entire troposphere and stratosphere. We used the temperature, the

119 geopotential height, and the specific humidity provided by the ERA-Interim pressure

120 levels data, and the discretised form of equation (1), to calculate the ZWD for each level

121 height (Böhm and Schuh, 2013):

122
$$
\begin{cases}
e_i = q_i \times P_i / (0.622 + 0.378 \times q_i) \\
N_{w_i} = k_2' \dfrac{e_i}{T_i} + k_3 \dfrac{e_i}{T_i^2} \\
ZWD = 10^{-6} \sum_i^{36} \dfrac{N_{w_i} + N_{w_{i+1}}}{2} \cdot \left(h_{i+1} - h_i \right)
\end{cases}
\tag{2}
$$

123 In equation (2), q is the specific humidity in g/g; P is the pressure in hPa; k_2' and k_3

124 are empirical constants same as equation (1); h is the geopotential height in meters.

125 From equation (2), we can see that the ZWD at specific level height is the sum of the

126 ZWD portions in all layers above the specific level height. Figure 1 shows the water

127 vapour pressure and ZWD profiles at a grid point ($0\degree$ N, $0\degree$ E) at 12:00 UTC on 1

128 January, 2010. From Figure 1, it can be seen that the downward trend in the water

129 vapour pressure varies significantly with height, and the decrease factor is different

130 across different height intervals. The changes in ZWD with respect to height are similar

131 to that of the water vapour pressure with respect to height: the decay is fastest up to a

132 few kilometres height and slows down with increasing height; the ZWD values are close

133 to zero after 10 km. Zhao *et al.* (2014) showed that about 50% of the water vapour

134 content is concentrated within 1.5 km of the surface and less than 10% of the water

135 vapour content remains above 5 km, leading to different ZWD decay rates within

136 different height intervals. These results are basically consistent with our experiment

137 results. Further, the derivative of the ZWD with respect to height (*i.e.*, ZWD vertical

138 gradient) is analyzed to better understand the characteristic of the ZWD vertical

139 distributions. Figure 2a shows the variation of ZWD vertical gradients with respect to

140 height at the same grid point to Figure 1. From Figure 2a, it can be seen that the trends

141 in ZWD vertical gradients at different height intervals are clearly different. Specifically,

142 the linear fit of the ZWD gradients with height below 2 km shows a great agreement

143 with an R square value of 0.99 (Figure 2b). Thus we can come to a conclusion: ZWD

144 gradients roughly change linearly below 2 km; and from 2 km to 5 km, and 5 km to 10

145 km, the ZWD gradients vary non-linearly.

146
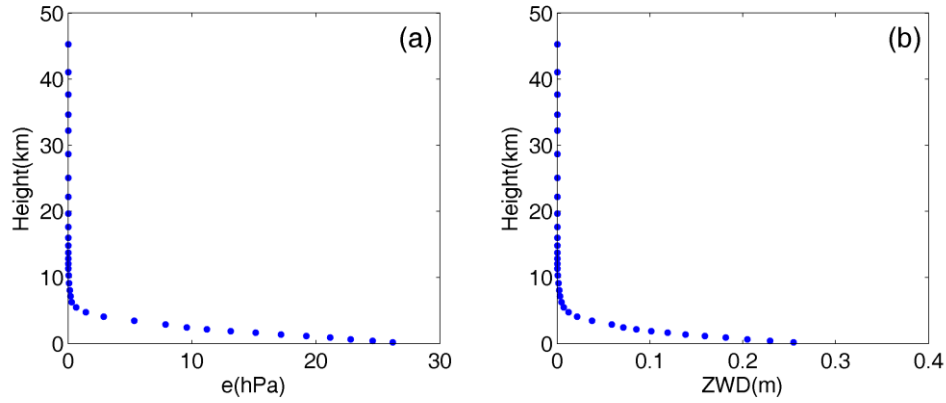
147 Figure 1 Water vapour pressure profile (a) and ZWD profile (b) at a grid point (0 °N, 0 °E) at

148 12:00 UTC on 1 January, 2010.

149
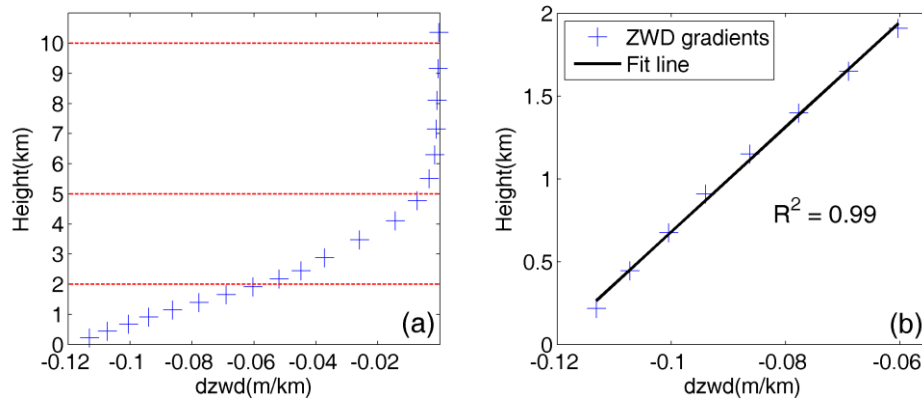
150 Figure 2 ZWD vertical gradients profile (a) and linear fit with height below 2 km (b) at a grid

151 point (0 °N, 0 °E) at 12:00 UTC on 1 January, 2010.

152 Figure 3 shows the ZWD vertical gradients with respect to height at grid points in

153 different latitude bands. Figure 4 shows the similar ZWD vertical gradients as Figure 3

154 but for different season. The variations are similar to those in Figure 2a, which show

155 trend changes at about 2 km and 5 km. It is worth noting that the ZWD gradients at low

156 latitudes are much larger and water vapour is more variable than at high latitudes,

157 resulting from the fact that the water vapour at low latitudes are more variable. In

158   addition, the ZWD gradient trends in the southern hemisphere are significant. In

159   contrast, the ZWD gradients in the northern hemisphere are slightly complicated with

160   respect to height: the reason for this may be that the southern hemisphere is mostly

161   oceanic while the northern hemisphere has many seacoasts. The terrain complexity in

162   the northern hemisphere contributes to the disturbances in the ZWD gradient in specific

163   areas. According to the vertical variation characteristics of ZWD, we divided the

164   troposphere into three height intervals: below 2 km, 2 km to 5 km, and 5 km to 10 km,

165   and assumed 10 km as the empirical tropopause beyond which the ZWD is assumed to

166   be zero. For ZWD fitting with respect to height, TropGrid2 and GPT2w use exponential

167   functions, while some scholars have also used a polynomial to describe the tropospheric

168   delay with respect to height (Song *et al*., 2011). We used both polynomial and

169   exponential functions to fit the variation trend of the ZWD with respect to height in the

170   three selected intervals, respectively. The results showed that the quadratic polynomial

171   used under 2 km, and exponential functions between 2 km and 5 km, and 5 km to 10

172   km gave the best fits. The combination of the quadratic polynomial and exponential

173   functions for different height intervals is termed piecewise height functions. Table 1

174   summarises the global fitting statistics of different fit functions, demonstrating the

175   superiority of piecewise height functions to the single polynomial function and single

176   exponential function used for the whole troposphere.

177
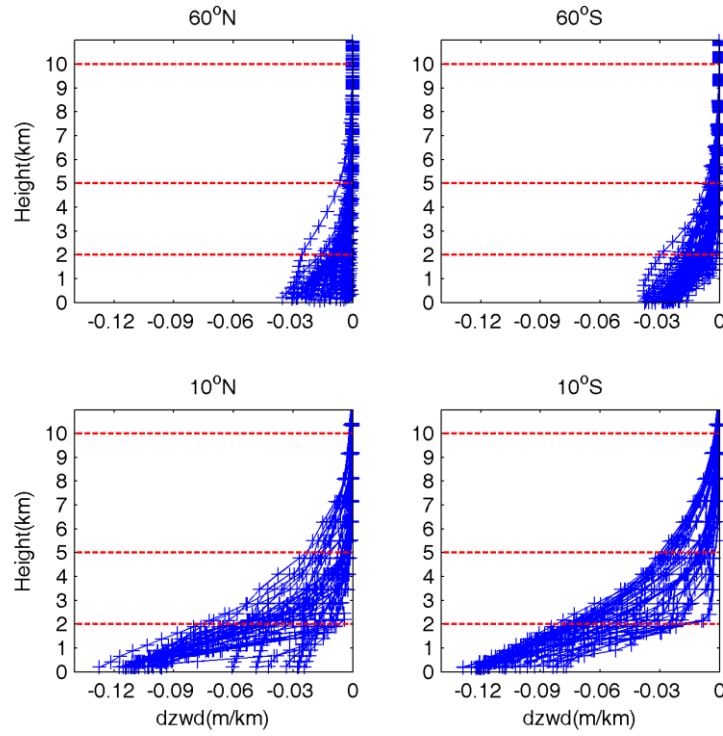
178   Figure 3 ZWD gradients profiles at grid points in different latitude bands (12:00 UTC, 1 January,

179   2010).

180
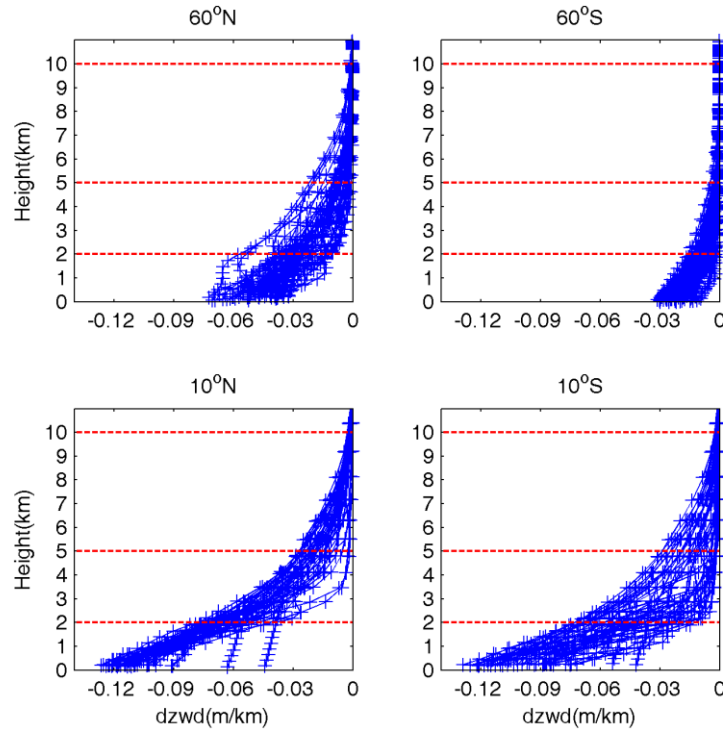
181   Figure 4 ZWD gradients profiles at grid points in different latitude bands (12:00 UTC, 1 July,

182   2010).

183

184 Table 1. Fitting RMSs of piecewise height functions, single quadratic polynomial function, and

185 single exponential function (unit: mm).

	< 2 km	2 km to 5 km	5 km to 10 km
Piecewise height functions	0.2	1.0	0.2
Quadratic polynomial	5.9	3.8	6.5
Exponential	2.3	2.2	1.0

186

3 The HZWD model

188   From the above analysis of ZWD vertical variation and fitting, the piecewise height

189 functions of the proposed HZWD model are:

$$
ZWD(B,L,H) = \begin{cases} z_1 + a_1 \cdot H + a_2 \cdot H^2 & H < 2000\ m \\ z_2 \cdot \exp\{\beta_2 \cdot (H-2000)\} & 2000\ m \le H < 5000\ m \\ z_3 \cdot \exp\{\beta_3 \cdot (H-5000)\} & 5000\ m \le H \le 10000\ m \\ 0 & H > 10000\ m \end{cases} \quad (3)
$$

191   In equation (3), B is the latitude in degrees; L is the longitude in degrees; H is the

192 height in meters; function coefficients z_1, z_2 and z_3 can be regarded as the ZWD at

193 the height of 0 km, 2 km and 5 km, respectively. We used the monthly mean profiles of

194 ERA-Interim pressure levels from 2001 to 2010 with a horizontal resolution of $5\,°\times5\,°$

195 for ZWD modelling. The ZWD profiles calculated for each grid point are fitted by

196 equation (3) to obtain the time series of the corresponding function coefficients: z_1,

197 a_1, a_2, z_2, β_2, z_3, and β_3. It is worth noting that the ERA-Interim-derived ZWD

198 data indicate that the averaged ZWD values at the three height intervals (*i.e.*, below 2

199 km, 2 km to 5 km, and 5 km to 10 km) are 0.126 m, 0.0489 m, and 0.0111 m,

200 respectively. Jin *et al*. (2007) found that the tropospheric delay has notable seasonal

201 variations, mainly on annual and semi-annual cycles. Song *et al*. (2011) and Zhao *et al*.

202 (2014) considered the temporal features of function coefficients in their troposphere

203 models. We used the ten-year time series of those coefficients obtained to analyse their

204   temporal variations. Figure 5 shows the time series and cycle fitting results of the

205   function coefficients z_1, z_2, and z_3 at grid point (0°N, 0°E). Figure 5 shows that

206   the time series of the function coefficients z_1, z_2, and z_3 have a significant

207   characteristic annual cycle, and the semi-annual cycle is small but nevertheless evident.

208
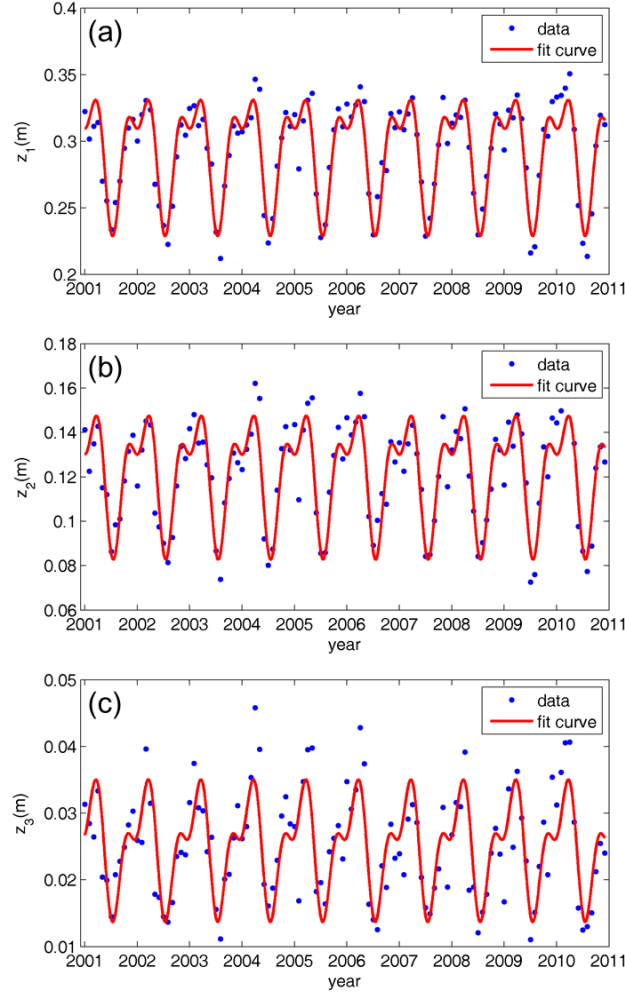
209   Figure 5 Decadal time series and cycle fitting results of function coefficients z_1 (a), z_2 (b), and

210   z_3 (c) at a grid point (0°N, 0°E) from 2001 to 2010.

211   Therefore, taking the annual, and semi-annual cycles into consideration, we used

212   equation (4) to fit the function coefficients derived from equation (3) to temporal

213   parameters for each grid point (Böhm *et al.*, 2015):

$$r(t) = A_0 + A_1 \cos\left(\frac{doy}{365.25} 2\pi\right) + B_1 \sin\left(\frac{doy}{365.25} 2\pi\right)$$
$$+ A_2 \cos\left(\frac{doy}{365.25} 4\pi\right) + B_2 \sin\left(\frac{doy}{365.25} 4\pi\right)$$

(4)

In equation (4), A_0 is the annual mean; A_1 and B_1 are the annual cycle parameters; A_2 and B_2 are the semi-annual cycle parameters; and *doy* is the day of the year. The fittings show that the annual means, and annual, and semi-annual amplitudes of z_1, z_2 and z_3 are distinct. For instance, the cycle fitting results at a grid (0 °N, 0 °E) (Figure 5) indicate that the temporal parameters (*i.e.*, A_0, A_1, B_1, A_2, and B_2) of z_1 are 0.2911 m, 0.0237 m, 0.0312 m, -0.0006 m, and -0.0227 m, respectively; the temporal parameters of z_2 are 0.1215 m, 0.0118 m, 0.0203 m, 0.0004 m, and -0.0146 m, respectively; the temporal parameters of z_3 are 0.0255 m, 0.00031 m, 0.0070 m, -0.0019 m, and -0.0044 m, respectively. It should be noted that the fitting results of coefficients a_2, β_2, and β_3 show that all their annual means, and annual, and semi-annual amplitudes are small. However, below 2 km, the lack of cycle terms in a_2 would cause centimetre level error in the ZWD estimates, so these terms have been retained. For β_2 and β_3, ZWD itself is small at heights above 2 km, so the annual mean suffices for a desirable ZWD estimate. The experiment reveals that the loss of accuracy due to the lack of annual and semi-annual terms in β_2 and β_3 for the ZWD estimates is less than 0.1 mm. Therefore, only the annual means are retained for these two coefficients.

Figure 6 shows the global distributions of annual means of model coefficients z_1, z_2, and z_3. From Figure 6 we can see that the extremum of ZWD annual means at 0 m height occur near the equator and the maximum exceeds 0.36 m. The ZWD annual means decrease with increasing latitude. The distributions of ZWD annual means at 2 km and 5 km heights are similar to that at 0 m, but the areas with the large values near

237   the equator decrease in extent and the ZWD distributions tend to be uniform, indicating

238   that the water vapour content near the equator is greater than that in other regions, and

239   the ZWD value is also larger in low altitude regions. As the height increases, the

240   difference in water vapour content or ZWD, between the equator and other areas begins

241   to decrease, but remains significant. Overall, there are some differences in the ZWD

242   distribution at different heights, and it is necessary to model the spatio-temporal

243   variations of ZWD at different heights.

244
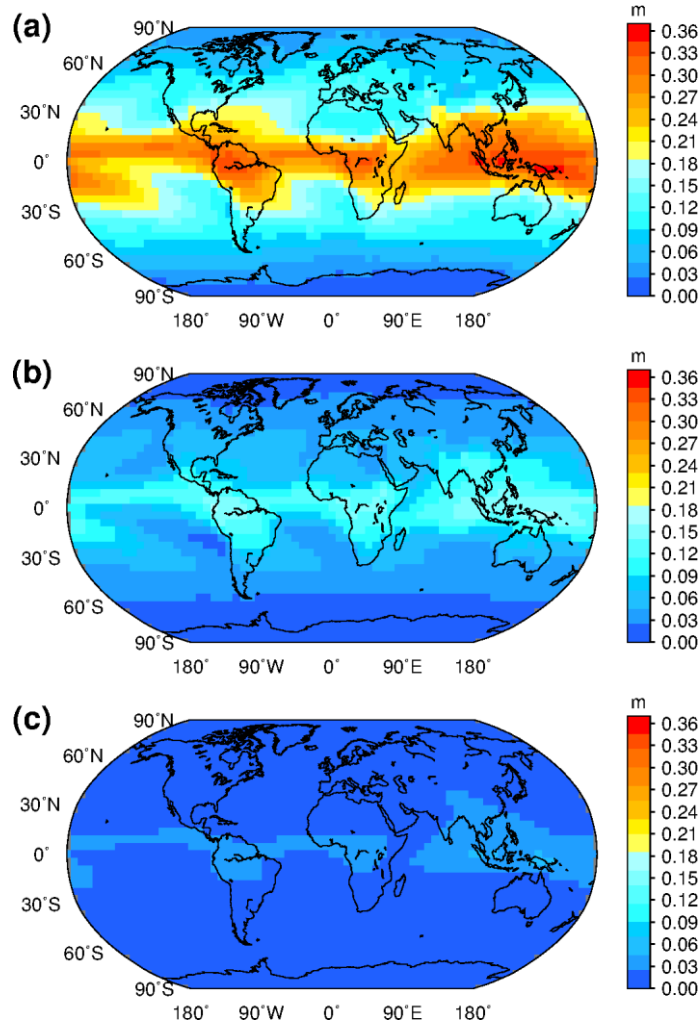
245   Figure 6 Global distributions of annual means of HZWD model coefficients z_1 (a), z_2 (b),

246   and z_3 (c).

247   After the fitting processes involving equations (3) and (4), the global ZWD model

248   HZWD, using piecewise height functions, is established. The spatial resolution of the

249   HZWD model is $5°\times5°$. Each grid point contains 7 primary coefficients: z_1, a_1, a_2,

z_2, β_2, z_3, and β_2. Among these coefficients, z_1, z_2, z_3, a_1, and a_2 are further expressed by equation (4) with 5 temporal parameters, respectively. Therefore, there are 27 parameters for each grid point and total 68094 parameters for the HZWD model. As a comparison, the GPT2w model has a number of 77760 parameters, which is 14% more than that of the HZWD model. It is worth noting that the UNB3m model only has 50 parameters due to its coarse spatio-temporal resolution. As with the UNB3m model and GPT2w model, the proposed HZWD model only needs the time and coordinates (latitude, longitude, and height) as input to estimate the ZWD. Compared with the UNB3m and GPT2w models, the unique characteristics of the HZWD model is the height interval divisions with piecewise functions. When the HZWD model is applied, the four grid points surrounding the station are determined according to the horizontal position (latitude and longitude) of the station, and then the model coefficients of the corresponding height intervals at the four selected points are calculated according to equation (4). The ZWD of the four grid points are extrapolated to the station height by using equation (3), and finally the ZWD at the station location is obtained by using bilinear interpolation. The HZWD model only needs time, latitude, longitude, and height as input parameters. It can calculate ZWD without meteorological data, and can provide wet delay correction products for navigation and positioning at different heights.

4 Validation and analysis of the HZWD model

To test the precision of HZWD model and analyse the model correction performance compared to other troposphere models, we used the ERA-Interim pressure levels data and radiosonde data from the year 2015 as external data sources, and compared the results with the commonly used models UNB3m and GPT2w. The parameters used for the validation are bias and root mean square (RMS) error expressed as:

$$bias = \frac{1}{n}\sum_{i=1}^{n}(ZWD_i^M - ZWD_i^0) \tag{5}$$

$$RMS = \sqrt{\frac{1}{n}\sum_{i=1}^{n}(ZWD_i^M - ZWD_i^0)^2} \tag{6}$$

278   In equation (5) and (6), ZWD_i^M is the value estimated by the HZWD model

279   developed in this study and ZWD_i^0 is the reference value.

280   For the UNB3m model, the ZWD at mean sea level (MSL) is first calculated, then

281   a vertical correction is applied to transform the ZWD to the target height. The formulae

282   are (Leandro et al., 2006):

283
$$\begin{cases} ZWD_0 = 10^{-6} \dfrac{(T_m k_2' + k_3)R_d}{g_m(\lambda+1) - \gamma R_d} \cdot \dfrac{e_0}{T_0} \\ ZWD = ZWD_0 \left(1 - \dfrac{\gamma H}{T_0}\right)^{\frac{(\lambda+1)g}{\gamma R_d} - 1} \end{cases} \tag{7}$$

284   where e_0, T_0, and ZWD_0 are the water vapour pressure, temperature and ZWD at

285   MSL, respectively; R_d is the specific gas constant for dry air (278.054 J kg^{-1} K^{-1});

286   γ and λ are the temperature lapse rate and water vapour decrease factor,

287   respectively; g_m is the gravity acceleration at the mass centre of the vertical column

288   of the atmosphere and can be computed with geodetic latitude φ and height h by:

289
$$g_m = 9.784\left(1 - 0.00266\cos 2\varphi - 0.28 \cdot 10^{-6} h\right) \tag{8}$$

290   T_m is the weighted mean temperature computed by:

291
$$T_m = T_0\left(1 - \frac{\gamma R_d}{g_m(\lambda+1)}\right) \tag{9}$$

292   For the GPT2w model, the modelled meteorological parameters at the four grid

293   points surrounding the target location are extrapolated vertically to the desired height,

294   then the Askne and Nordius formula (10) is used to calculate the wet delays at those

295   base points: finally the wet delays are interpolated to the observation site in horizontal

296   direction to get the target ZWD.

297
$$ZWD = 10^{-6} \cdot (k_2' + \frac{k_3}{T_m}) \cdot \frac{R_d e}{(\lambda+1)g_m} \tag{10}$$

298   In GPT2w model, T_m is an empirical parameter modelled with seasonal

299   components and g_m is simplified to a constant (9.80665 m s^{-2}). It should be noted that

300   the GPT2w model provides both $1°\times1°$ and $5°\times5°$ resolution versions. Since the

301   horizontal resolution of HZWD model is $5°\times5°$, we used the GPT2w model with the

302   same resolution for validation.

303   **4.1 Validation with ECMWF data**

304   Modelling of the HZWD model is based on the monthly mean profiles of ERA-

305   Interim pressure levels data from 2001 to 2010, while we used the ERA-Interim

306   pressure levels data with the full time resolution of 6 hours in 2015 for the model

307   validation. This is to validate the model performance on the daily scale. Regarding the

308   ZWD profiles calculated from these data as reference values, we calculated the global

309   annual average bias and RMS error of the ZWD for three models (HZWD, GPT2w, and

310   UNB3m) within the three height intervals: below 2 km, 2 km to 5 km, and 5 km to

311   10 km (Table 2).

312   Table 2 Error statistics for the three models compared to the 2015 ECMWF data (unit: mm).

	< 2 km		2 km to 5 km		5 km to 10 km	
	bias	RMS	bias	RMS	bias	RMS
HZWD	-2.0	23.8	-1.4	13.1	0.0	2.6
GPT2w	-0.1	25.2	2.5	14.0	2.2	3.8
UNB3m	16.6	41.4	10.9	22.7	3.5	5.8

313   From Table 2, it can be seen that the HZWD model is the most accurate model

314   across all three intervals, followed by the GPT2w model, and the UNB3m model has

315   the worst performance. The annual average biases of the HZWD model are lower than

316   that of the GPT2w model and the UNB3m model except below 2 km. Compared with

317   the RMS errors in the GPT2w model, those of the HZWD model are decreased by 1.4

318   mm, 0.9 mm, and 1.2 mm within the three height intervals, corresponding to

319   improvements of about 6%, 6%, and 32%, respectively. The improvements of HZWD

320   model over GPT2w model will result in precision improvements of 2.8 mm, 1.8 mm,

321   and 2.4 mm respectively in height estimates in the positioning. The correction

322   performance improvement from 5 km to 10 km height is particularly evident. Figure 7a

323 shows the ECMWF ZWD profile and the ZWD profiles of the three models at 12:00

324 UTC on 1 January, 2015 at a representative grid point (0 ° N, 20 ° E). More clearly,

325 Figure 7b shows the differences between the ZWD profiles of the three models and

326 ECMWF ZWD profile at different heights. It can be seen that HZWD is the most stable

327 model, showing the best agreement with the ECMWF ZWD data, which is superior to

328 both the GPT2w, and the UNB3m, models.

329

330
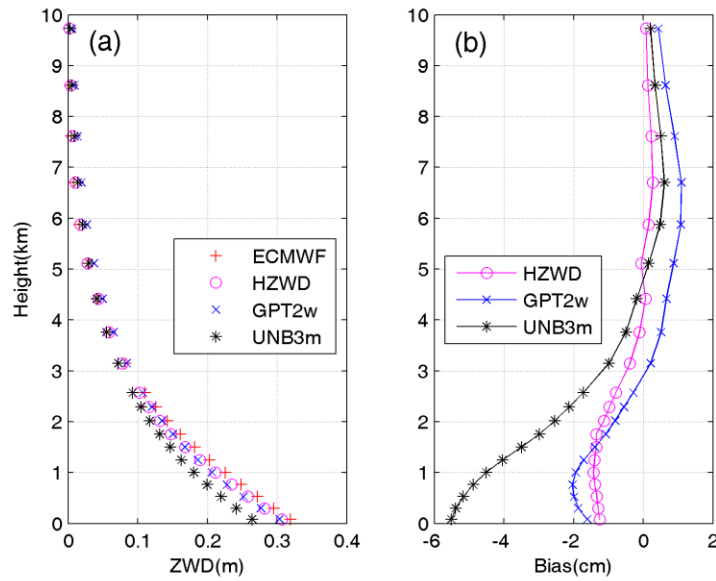
331 Figure 7 The ZWD profiles (a) of ECMWF and the three models (HZWD, GPT2w, and UNB3m)

332 and corresponding biases (b) at a grid point (0 °N, 20 °E) at 12:00 UTC on 1 January, 2015.

333 The variation of the troposphere has a strong correlation with latitude. To analyse

334 the correction performances of the three models in different regions around the world,

335 we calculated the three models' errors in different latitude bands (10 °intervals). Figures

336 8 and 9 show the correction performances at different latitudes. It can be seen from

337 Figure 8 that the bias of the UNB3m model is basically positive in the three height

338 intervals, indicating that its ZWD estimates are relatively large compared to the

339 ECMWF data. Moreover, the bias in the southern hemisphere is significantly larger than

340 that in the northern hemisphere, indicating systematic deviations in the southern

341 hemisphere. Both the GPT2w model and the HZWD model have large biases in the low

342 latitudes. The biases of the GPT2w model are positive from 2 km to 5 km and 5 km to

343 10 km height, indicating that the ZWD is overestimated by the GPT2w model with

increasing height. For the HZWD model, the bias in each latitude band is relatively small with few exceptions, resulting in a global average bias close to zero (see Table 2).

Figure 9 shows the RMS errors of the three models. It can be seen from Figure 9 that the precision of HZWD model is significantly better than that of the UNB3m model across the three height intervals and all latitude bands, which is better than GPT2w model in general. The precision of the three models declines with decreasing latitude, because the active change of water vapour in these areas limits the precision of the model. Corresponding to Figure 8, the errors in UNB3m are asymmetric: the main reason for this is that the meteorological parameters of UNB3m are interpolated from the coarse look-up table with a latitude interval of 15 ° and UNB3m does not consider the longitudinal variations of any meteorological elements. It should be pointed out that the UNB3m model is based on the simple symmetric assumption of the northern and southern hemispheres, and its modelling data source only comes from the atmospheric data collected over North America, which leads to poor precision in the southern hemisphere, especially in the high latitudes thereof.

Summarising the distributions of bias and RMS error across different latitude bands, we can see that the HZWD model performs best with the ECMWF data as reference values. Compared with the models GPT2w and UNB3m, the HZWD model basically eliminates systematic error in the 5 km to 10 km height interval and the correction performance is stable at all heights and regions. To investigate the model's performance over time, the Figure 10 shows the time series of RMSs for the three models at 6-hour intervals throughout the year 2015 at grid point (0 °N, 20 °E). We can see that the HZWD model has the best overall performances within the three height intervals over the year 2015. We noticed the significantly large RMSs for all three models across all three height intervals around the doy 19 and doy 195 of 2015. This can be attributed to the sharp short-term ZWD variations in the equator area. The short-term variations are hardly accounted for by all three models which only consider the seasonal variations of ZWD. Moreover, the GPT2w model has the worst performance from 5 km to 10 km height, which is also identified by Figure 8 and Figure 9.

373
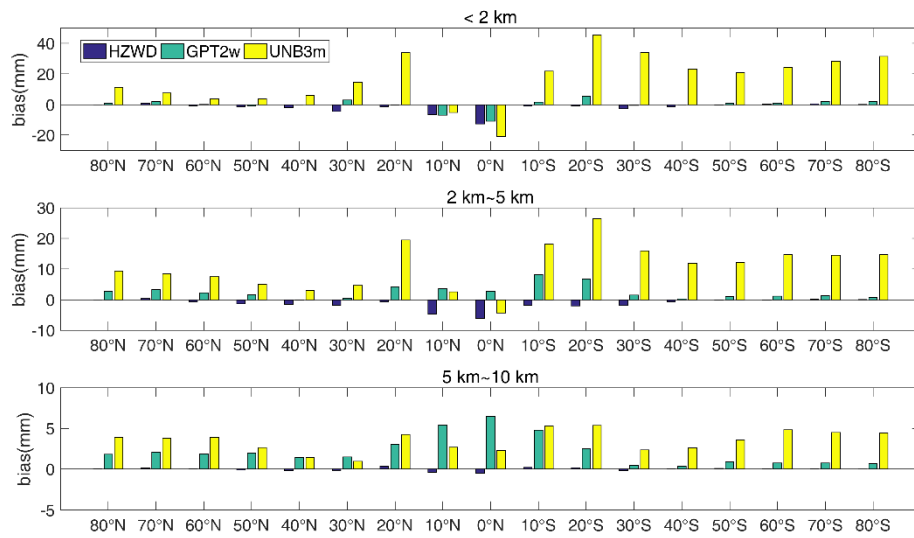
374   Figure 8 Bias comparisons between the three models (HZWD, GPT2w, and UNB3m) in different

375   latitude bands over the year 2015.

376
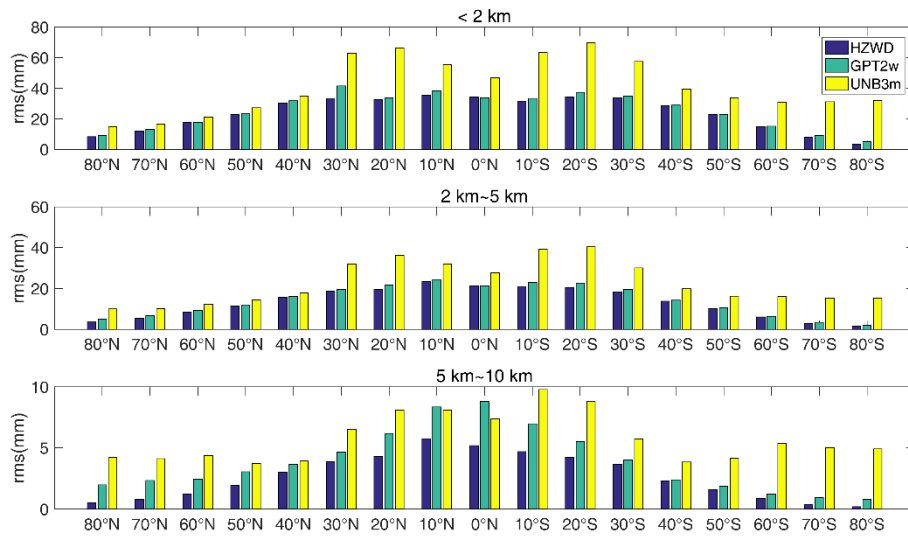
377   Figure 9 RMS error comparisons between the three models (HZWD, GPT2w, and UNB3m) in

378   different latitude bands over the year 2015.

379

380
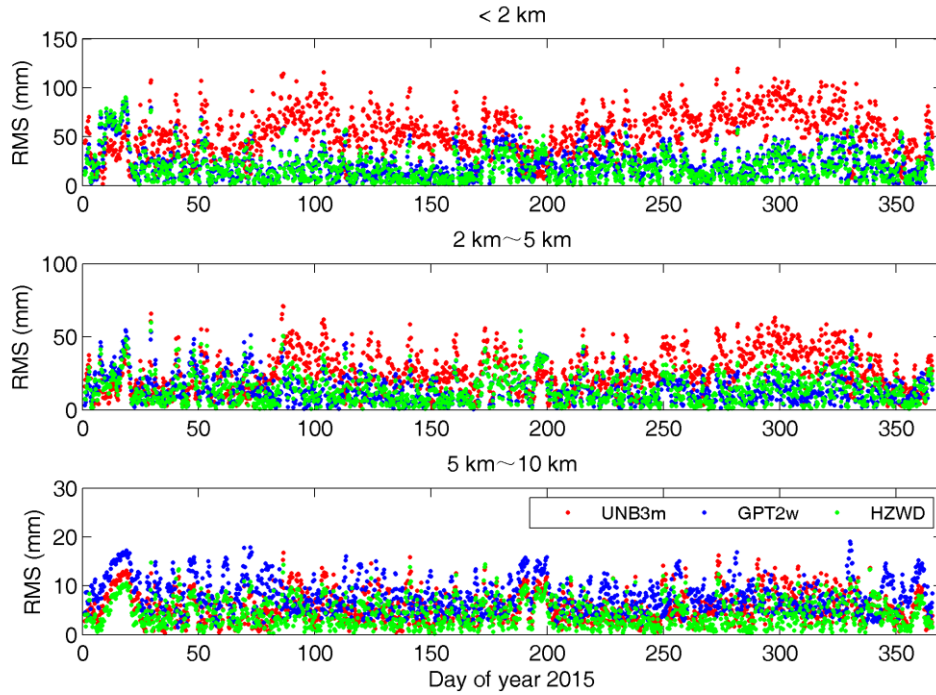
381 Figure 10 RMS errors in ZWD estimates of the three models (HZWD, GPT2w, and UNB3m)

382 compared to the ECMWF data over the year 2015 at grid point (0 °N, 20 °E).

383

4.2 Validation with radiosonde data

385   A radiosonde is used in a sounding technique that regularly releases balloons to

386 collect atmospheric meteorological data at different heights: it can obtain profiles of

387 various meteorological data with high accuracy. At present, the Integrated Global

388 Radiosonde Archive (IGRA) website (ftp://ftp.ncdc.noaa.gov/pub/data/igra/) provides

389 free downloads of global radiosonde data. We used radiosonde data from 318 stations

390 collected in 2015 to test the HZWD model. After data pre-processing, the data with

391 gross errors have been removed and a total of 163,671 radiosonde data epochs remained.

392 With the provided profiles of geopotential height, temperature, and water vapour

393 pressure, the data form of the radiosonde data are very similar to the ECMWF pressure

394 level data, thus the radiosonde ZWDs can be calculated using the same method by

395 equation (2). Before the validation, we conducted an assessment of the uncertainty of

396 ZWD derived from radiosonde data. Rozsa (2014) showed that the uncertainty of ZWD

397 is ± 1.5 mm in case of the Vaisala RS-92 radiosondes in Central and Eastern Europe.

398 However, this uncertainty is only valid for the ZWD calculated from the height of

399 lowest layer and is limited to Europe area. Using the same uncertainties of radiosonde

400 meteorological data given by the technical specification of the radiosonde (Vaisala 2010)

401 and the algorithm proposed by Rozsa (2014), we calculated the ZWD uncertainty for

402 all heights in all radiosonde stations. Figure 11 shows the uncertainty of ZWD with

403 respect to the height for radiosonde station 01241 located in Orland, Norway

404 (63.70 °N/9.60 °E/10 m). We can see that the uncertainty of ZWD is less than ±1.5 mm

405 near height of 0 m and decrease quickly with increasing height. The global mean

406 uncertainties of ZWD of all stations in the three height intervals are ±1.3 mm, ±0.7

407 mm and ±0.2 mm, respectively, indicating the high accuracy of ZWD derived from

408 radiosonde data.

409

410

411 Figure 11 Uncertainty of ZWD with respect to height at station 01241 (63.70 °N/9.60 °E/10 m)

412 at 11:00 UTC on January 1, 2015.

413 Taking the radiosonde ZWDs as reference ZWD values, we validated the ZWDs

414 from models HZWD, GPT2w and UNB3m. Table 3 shows the statistical results of the

415 three models. It can be seen from Table 3 that the HZWD model has the best overall

416 stability of the average bias and RMS error indicating the best precision, and the

417 UNB3m model is the worst. Compared with the GPT2w model, the RMS errors in

418 HZWD in the three height intervals are reduced by 0.6 mm, 0.9 mm, and 1.7 mm, which

419 equates to precision improvements of 2%, 5%, and 33%, respectively. Moreover, these

420 improvements correspond to the error reduces of 1.2 mm, 1.8 mm, and 3.4 mm

421 respectively in height estimates in geodetic techniques. Taking the uncertainty of

422 radiosonde ZWD into account, the improvement of HZWD model over GPT2w model

423 below 2 km seem to be insignificant. Nevertheless, we can reasonably think that the

424 ZWD predicted by HZWD is closer to true ZWD due to its smaller RMS error. It is

425 worth noting that the bias and RMS error of the HZWD model and the GPT2w model

426 are both larger than those of the results from ECMWF data in Table 2. The reason is

427 that the HZWD model and the GPT2w model are based on ECMWF data, thus the test

428 results with radiosonde data are slightly worse than those using ECMWF data. On the

429 contrary, the bias of the UNB3m model decreases, and the RMS error between 2 km

430 and 5 km, and 5 km and 10 km, are less than those in Table 2. It may be due to the fact

431 that most of the radiosonde stations are in the northern hemisphere, accounting for more

432 than 60% (192/318) of the total, which has a positive impact on the test results for

433 UNB3m model based on North American meteorological data.

434 Figure 12 shows the global distributions of bias for the three models within the

435 three height intervals, and Figure 13 shows the global distributions of RMS error for

436 the three models. As can be seen from Figure 12, the three models show a poorer

437 performance in low-latitude areas than in mid- and high-latitude areas for all height

438 intervals, similar to the results of in Section 4.1. Within the 5 km to 10 km interval, the

439 bias of the GPT2w model is large and positive in the equatorial region, indicating that

440 the ZWD of the GPT2w in this height is significantly overestimated, and the global bias

441 of the UNB3m model in this height interval is positive, also indicating an overestimate

442 of the ZWD in the UNB3m model. The bias of the HZWD model does not show obvious

443 regional differences with respect to height, and the overall distribution of HZWD model

444 bias has no tendency to either the positive or negative. Figure 13 further illustrates the

445 precision of the HZWD model. The global RMS error distributions of HZWD model

446 are similar to that of GPT2w model below 2 km and between 2 km and 5 km, but the

447 precision of the HZWD model is slightly better. Combining this with the bias

448 distribution of the GPT2w model in Figure 12, the GPT2w model also has a large RMS

449 error near the equator in the 5 km to 10 km interval, which shows that the GPT2w model

450 is unstable at high height in low-latitude areas. The precision of the UNB3m model is

451 poorer than that of both the HZWD, and GPT2w, models. Below 2 km, the UNB3m

452 model reaches decimetre-level precision near the equator, and even exceeds 12 cm in

453 some areas: the distribution of north-south heterogeneity remains obvious.

454 Table 3 Error statistics for the three models validated by 2015 radiosonde data (unit: mm).

	< 2 km		2 km to 5 km		5 km to 10 km	
	bias	RMS	bias	RMS	bias	RMS
HZWD	-3.6	30.1	-2.0	15.8	0.1	3.5
GPT2w	-3.2	30.7	3.5	16.7	3.3	5.2
UNB3m	5.9	46.0	6.2	23.1	2.6	5.7

455

456
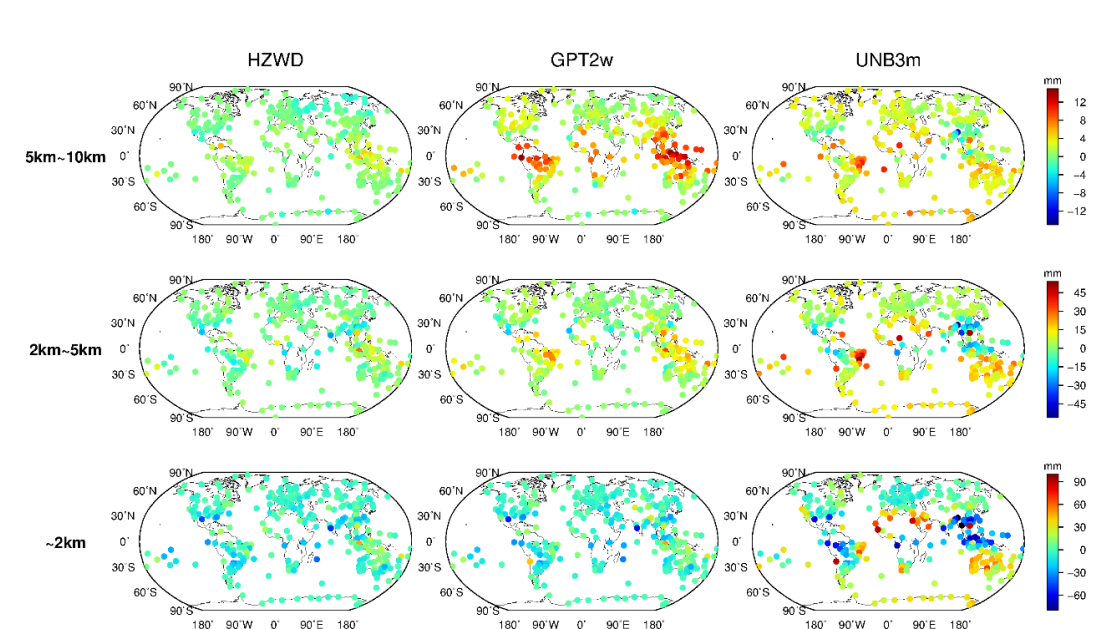
457 Figure 12 Global distributions of bias for the three models (HZWD, GPT2w, and UNB3m)

458 compared to 2015 radiosonde data.

Figure 13 Global distributions of RMS error for the three models (HZWD, GPT2w, and UNB3m) compared to 2015 radiosonde data.

These results validate the spatial stability of the precision of the HZWD model, furthermore the temporal stability of the model precision is verified next. Figure 14 shows the results of ZWD corrections of the three models for the radiosonde station 01241 for the whole of 2015. It can be seen from Figure 14 that the HZWD model and the GPT2w model are relatively stable throughout the year, while the correction performance of the UNB3m model in 2015 is worse than those of the HZWD and GPT2w models. The probable reason for this is that the UNB3m model only takes into account the annual variations in the metrological elements with a fixed phase, resulting in precision instability throughout the year. The improvement performance arising from use of the HZWD model, compared to that arising from use of the GPT2w model, is more apparent with increasing height: this shows that modelling ZWD piecewise with height can effectively approximate the real ZWD profile and improve the precision of ZWD estimation.

476
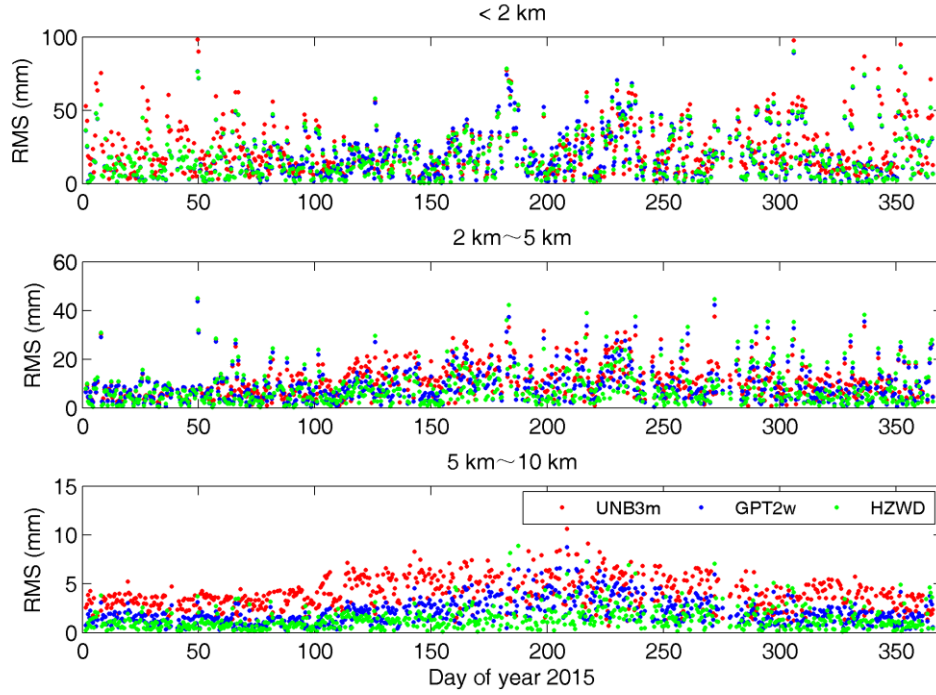
477   Figure 14 RMS errors in ZWD estimates of the three models (HZWD, GPT2w, and UNB3m)

478   for radiosonde station 01241 over the year 2015.

479

5 Conclusions

480

481   The complexity of spatio-temporal variations makes the modelling of tropospheric

482   ZWD difficult. In this paper, the characteristics of vertical variation of wet delay are

483   analysed. The troposphere is divided into three height intervals: below 2 km, 2 km to 5

484   km, and 5 km to 10 km according to different trends (10 km is assumed to represent the

485   empirical tropopause). A quadratic polynomial and two exponential functions are used

486   to describe the variation of wet delay within each of the three intervals. Based on the

487   monthly mean data of ECMWF ZWD from 2001 to 2010, a global ZWD model with

488   spatial resolution of $5\degree \times 5\degree$ was established with height fitting followed by periodic

489   fitting. Using the ECMWF ZWD data for 2015, the annual average RMS errors in the

490   HZWD model are 23.8 mm, 13.1 mm, and 2.6 mm in the below 2 km, 2 km to 5 km,

491   and 5 km to 10 km height intervals, respectively, which is far superior to the

492   performance of the UNB3m model. Compared to the currently most accurate wet delay

493   empirical model (the GPT2w model), the precisions within the three height intervals

improved by 6% (1.4 mm), 6% (0.9 mm), and 32% (1.2 mm), respectively. The improvements will result in precision improvements of 2.8 mm, 1.8 mm, and 2.4 mm respectively in height estimates in the positioning. The testing results of radiosonde data from 318 stations in 2015 show that the annual average RMS errors of the HZWD model are 30.1 mm, 15.8 mm, and 3.5 mm, which are 2% (0.6 mm), 5% (0.9 mm), and 33% (1.7 mm) better than those of the GPT2w model, respectively, corresponding to height error reduces of 1.2 mm, 1.8 mm, and 3.4 mm in the positioning. Considering the ZWD fields (0.126 m, 0.0489 m, and 0.0111 m) in the three height intervals, the precision improvements at the top layer are especially significant, which accounting for about 15% of the corresponding ZWD field. Moreover, compared with the GPT2w, and UNB3m, models, the HZWD model offers the highest spatio-temporal stability. With higher precision of ZWD estimates and less model parameters, the HZWD model is more efficient than the GPT2w model.

The HZWD model offers good precision stability in the vertical direction and can meet the requirements of ZWD correction at different heights within the troposphere; however, it can be seen that neither the HZWD, nor the GPT2w models, *i.e.*, those non-meteorological parameter-based models, performed well in the lowest region of the troposphere. In addition, compared with GPT2w, HZWD model is a closed model with a limitation to facilitate on-site meteorological observations. Further research is required to assess the variation and factors influencing of the wet delay and explore the possibility of incorporation of on-site meteorological data. Additionally, to enhance the model performance in real-time conditions, the potential of the incorporation of numerical weather forecasts data in the HZWD model will be explored in future research.

Acknowledgements: The authors would like to thank the ECMWF and IGRA for providing relevant data. This research was supported by the National Key Research and Development Program of China (2016YFB0501803) and the National Natural Science Foundation of China (41574028) and Key Laboratory of Geospace Environment and Geodesy, Ministry of Education, Wuhan University (16-02-03).

References

Askne, J., & Nordius, H. (1987). Estimation of tropospheric delay for microwaves from surface weather data. Radio Science, 22(3), 379-386.

Bevis, M., Businger, S., Chiswell, S., Herring, T. A., Anthes, R. A., Rocken, C., & Ware, R. H. (1994). GPS meteorology: Mapping zenith wet delays onto precipitable water. Journal of applied meteorology, 33(3), 379-386.

Böhm, J., & Schuh, H. (Eds.). (2013). Atmospheric effects in space geodesy (Vol. 5). Berlin: Springer.

Böhm, J., Möller, G., Schindelegger, M., Pain, G., & Weber, R. (2015). Development of an improved empirical model for slant delays in the troposphere (GPT2w). GPS Solutions, 19(3), 433-441.

Collins, P., Langley, R., & LaMance, J. (1996). Limiting factors in tropospheric propagation delay error modelling for GPS airborne navigation. Proc. Inst. Navig. 52nd Ann. Meet, 3.

Davis, J. L., Herring, T. A., Shapiro, I. I., Rogers, A. E. E., & Elgered, G. (1985). Geodesy by radio interferometry: Effects of atmospheric modeling errors on estimates of baseline length. Radio science, 20(6), 1593-1607.

Dee, D. P., Uppala, S. M., Simmons, A. J., Berrisford, P., Poli, P., Kobayashi, S., ... & Bechtold, P. (2011). The ERA‐Interim reanalysis: Configuration and performance of the data assimilation system. Quarterly Journal of the royal meteorological society, 137(656), 553-597.

Fernandes, M. J., Nunes, A. L., & Lázaro, C. (2013). Analysis and inter-calibration of wet path delay datasets to compute the wet tropospheric correction for CryoSat-2 over ocean. Remote Sensing, 5(10), 4977-5005.

Fernandes, M. J., Lázaro, C., Nunes, A. L., & Scharroo, R. (2014). Atmospheric corrections for altimetry studies over inland water. Remote Sensing, 6(6), 4952-4997.

Hobiger, T., Ichikawa, R., Koyama, Y., & Kondo, T. (2008). Fast and accurate ray‐tracing algorithms for real‐time space geodetic applications using numerical weather models. Journal of Geophysical Research: Atmospheres, 113(D20).

Hopfield, H. S. (1971). Tropospheric effect on electromagnetically measured range: Prediction from surface weather data. Radio Science, 6(3), 357-367.

553   Jin, S., Park, J. U., Cho, J. H., & Park, P. H. (2007). Seasonal variability of GPS‐derived zenith

554   tropospheric delay (1994‐2006) and climate implications. Journal of Geophysical Research:

555   Atmospheres (1984‐2012), 112(D9).

556   Kouba, J. (2008). Implementation and testing of the gridded Vienna Mapping Function 1 (VMF1).

557   Journal of Geodesy, 82(4-5), 193-205.

558   Krueger, E., Schueler, T., Hein, G. W., Martellucci, A., & Blarzino, G. (2004, May). Galileo

559   tropospheric correction approaches developed within GSTB-V1. In Proc. ENC-GNSS (Vol. 1619).

560   Krueger, E., Schueler, T., & Arbesser-Rastburg, B. (2005). The standard tropospheric correction

561   model for the European satellite navigation system Galileo. Proc. General Assembly URSI.

562   Lagler, K., Schindelegger, M., Böhm, J., Krásná, H., & Nilsson, T. (2013). GPT2: Empirical slant

563   delay model for radio space geodetic techniques. Geophysical research letters, 40(6), 1069-1073.

564   Leandro, R., Santos, M. C., & Langley, R. B. (2006, January). UNB neutral atmosphere models:

565   development and performance. In Proceedings of ION NTM (Vol. 52, No. 1, pp. 564-73).

566   Möller, G., Weber, R., & Böhm, J. (2014). Improved troposphere blind models based on numerical

567   weather data. Navigation, 61(3), 203-211.

568   Nafisi, V., Madzak, M., Böhm, J., Ardalan, A. A., & Schuh, H. (2012). Ray-traced tropospheric

569   delays in VLBI analysis. Radio Science, 47(02), 1-17.

570   Niell, A. E. (1996). Global mapping functions for the atmosphere delay at radio wavelengths.

571   Journal of Geophysical Research: Solid Earth, 101(B2), 3227-3246.

572   Nilsson, T., & Elgered, G. (2008). Long‐term trends in the atmospheric water vapor content

573   estimated from ground‐based GPS data. Journal of Geophysical Research: Atmospheres,

574   113(D19).

575   Rózsa S Z. Uncertainty considerations for the comparison of water vapour derived from radiosondes

576   and GNSS[M]//Earth on the Edge: Science for a Sustainable Planet. Springer Berlin Heidelberg,

577   2014: 65-78.

578   RTCA (2016), Minimum Operational Performance Standards For Global Positioning

579   System/Satellite-Based Augmentation System Airborne Equipment, Radio Technical Commission

580   for Aeronautics, SC-159, publication DO-229E, Washington, D. C.

581   Saastamoinen, J. (1972). Introduction to practical computation of astronomical refraction. Bulletin

582   Géodésique (1946-1975), 106(1), 383-397.

583   Schüler, T. (2014). The TropGrid2 standard tropospheric correction model. GPS solutions, 18(1),

584   123-131.

585   Song, S., Zhu, W., Chen, Q., & Liou, Y. (2011). Establishment of a new tropospheric delay

586   correction model over China area. Science China Physics, Mechanics and Astronomy, 54(12), 2271-

587   2283.

588   Stum, J., Sicard, P., Carrere, L., & Lambin, J. (2011). Using objective analysis of scanning

589   radiometer measurements to compute the water vapor path delay for altimetry. IEEE Transactions

590   on Geoscience and Remote Sensing, 49(9), 3211-3224.

591   Vieira, T., Fernandes, M. J., & Lázaro, C. (2017). Analysis and retrieval of tropospheric corrections

592   for cryosat-2 over inland waters. Advances in Space Research.

593   Zhao J Y, Song S L, Chen Q M, et al. (2014). Establishment of a new global model for zenith

594   tropospheric delay based on functional expression for its vertical profile. Chinese J. Geophys. (in

595   Chinese), 57(10), 3140-3153.

596